A Novel Power-Angle Control Method of DFIG-DC System Based on Regulating Air Gap Flux Vector

Chao Wu, *Member, IEEE*, Dao Zhou, *Senior Member, IEEE*, Peng Cheng, *Member, IEEE*, and Frede Blaabjerg, *Fellow, IEEE*

***Abstract*—This article presents a novel power-angle control method of the doubly fed induction generator dc system based on regulating the air gap flux vector. The relationship between the angle of air gap electromotive force (EMF) vector and the stator output power is revealed in this article, which can be used for controlling the output power directly. Since the stator frequency is determined by the rotating speed of air gap flux vector and the output power is determined by the angle of air gap EMF vector, the stator frequency can be generated by the power control loop that can avoid the classical voltage model or current model and reduce the parameter dependence. The stator frequency can be regulated through the *d*-axis rotor current since the product of the stator frequency and the *d*-axis rotor current is constant. Furthermore, the improved direct resonant control for torque ripple and harmonic current mitigation can still be applied in this novel control method because air gap flux orientation is achieved through controlling the *q*-axis air gap flux to be zero. Finally, the experimental results are presented to validate the proposed control method.**

***Index Terms*—Air gap flux vector, direct resonant control, doubly fed induction generator (DFIG), power-angle control.**

I. Introduction

RECENTLY, there are growing research interests in the direct current (dc) transmission and connection of doubly fed induction generator (DFIG) based wind farm [1]–[4]. In the multiple existing topologies of DFIG connected to dc grid, the DFIG connected to dc grid through diode bridge on the stator side has gained extensive attention and research due to its simple structure and smaller converter cost, which is also called as DFIG-dc system. However, the traditional vector control strategy based on the phase-locked loop (PLL) cannot be applied because there is no ac grid in the DFIG-dc topology and the stator frequency needs to be controlled additionally [5]. Thus, the primary objective of this topology is to achieve accurate control of the stator frequency and output power. However, the basic problem encountered of this topology is how to obtain the stator frequency and orientation angle with as little parameter dependence as possible.

There are several research articles devoting to studying the control strategies of this DFIG-dc system [6]–[15]. The decoupling control of stator frequency and stator power is mostly achieved through the stator flux orientation control. In these methods, the stator frequency and the stator flux angle are indispensable for the decoupling control. According to the methods of obtaining the stator frequency and orientation angle, these existing methods can be generally divided into two categories: voltage model or current model.

In [6]–[8], the stator frequency and the stator flux angle are obtained based on the stator voltage model. In [6] and [7], the stator frequency and the stator flux angle are directly calculated based on the stator flux, which is highly dependent on the resistance parameters. Furthermore, the stator flux is the integral of stator voltage, which is difficult to achieve in practical occasion due to an unavoidable dc sampling offset. In [8], the integral link is substituted by inertia link that can reduce the effect of dc sampling offset but cannot eliminate the effect of dc sampling offset, which will cause a fundamental frequency ripple in the orientation angle.

In [9]–[12], the stator frequency and the stator flux angle are acquired based on the current model. In [9], the magnitude of stator flux is applied for the stator frequency control, which is dependent on the stator inductance and mutual inductance. In [10]–[12], a stator flux PLL is proposed to obtain the stator frequency and the stator flux angle by controlling the *q*-axis stator flux to be zero, which can avoid the calculation process but also dependent on the ratio of stator inductance and mutual inductance. When the DFIG-dc system is operating in the standalone mode, the dc voltage is also controlled based on the stator flux orientation [13]–[15].

In conclusion, all these existing methods based on the stator flux orientation control cannot avoid the dc offset issue or parameter dependence. It can be found that there is no ac grid imposed on the stator side of DFIG and there is no reactive power flow to the dc grid; thus, the stator flux orientation control and the decoupling control of stator frequency and stator power are not necessary for this topology.

Totally different from the existing DFIG-dc control methods, the stator frequency and the stator power are not decoupling

Manuscript received October 9, 2019; revised February 18, 2020; accepted June 10, 2020. Date of publication June 11, 2020; date of current version September 4, 2020. This work was supported in part by THE VELUX FOUNDATIONS under the VILLUM Investigator Grant REPEPS under Award 00016591 and in part by the National Natural Science Foundation of China under Grant 51807182. Recommended for publication by Associate Editor J. Clare. *(Corresponding author: Peng Cheng.)*

Chao Wu, Dao Zhou, and Frede Blaabjerg are with the Department of Energy Technology, Aalborg University, 9220 Aalborg, Denmark (e-mail: cwu@et.aau.dk; zda@et.aau.dk; fbl@et.aau.dk).

Peng Cheng is with the China Institute of Energy and Transportation Integrated Development, North China Electric Power University, Beijing 102206, China (e-mail: p.cheng@ncepu.edu.cn).

Color versions of one or more of the figures in this article are available online at https://ieeexplore.ieee.org.

Digital Object Identifier 10.1109/TPEL.2020.3001967

control through the *d–q* axis rotor current. The relationship between the stator power and angle of air gap electromotive force (EMF) is established. The stator power is not controlled by the rotor current on the active axis but controlled by the angle between the air gap voltage and the stator-side voltage. In this way, the stator frequency and the orientation angle are obtained based on the stator active power control loop, which can avoid the voltage model and the current model. Furthermore, the air gap flux orientation method is achieved by controlling the *q*-axis exciting current to zero. Through regulating the air gap flux vector, the stator frequency and the stator active power can both be controlled accurately without parameter dependence and avoid the sampling offset problem.

Since the stator voltage is highly distorted, the harmonic currents will cause torque ripple, which should be reduced. In [16] and [17], predictive control methods are proposed for suppressing torque ripples. However, these kinds of literature are just aimed at the torque ripple suppression without considering the harmonic currents in the stator and rotor winding. An improved direct resonant control method is proposed for suppressing the torque ripples and mitigating harmonic currents simultaneously [18]. In this article, since the rotating frame is aligned with the air gap flux vector, the improved direct resonant control method is still suitable in this novel control method, which can mitigate the torque ripple and harmonic currents simultaneously.

In conclusion, the novel frequency and power control method can avoid the parameter dependence. Moreover, all the existing direct resonant control for improving the performance can still be applied directly.

The rest of the article is organized as follows. The system configuration and the mathematical model are described in Section II. The detailed control strategy of the rotor-side converter (RSC) is elaborated in detail in Section III. Furthermore, the performance analysis of power-angle control and improved direct resonant control is presented in Section IV. Section V shows the experimental. Finally, Section VI concludes the article.

II. System Configuration and Mathematical Model

A. System Configuration

The DFIG-dc system topology is graphically shown as Fig. 1, where U_{sabc} represents the stator voltage, $V_{\rm dc}$ represents the dc-link voltage, and $i_{\rm dc}$ represents the dc-side current. The working principle of DFIG to generate power to the dc grid can be elaborated as follows. First, the rotor-side exciting current is injected to the rotor winding through RSC, then the air gap EMF is built. When the peak value of the phase–phase air gap EMF is higher than the dc voltage, the diode bridge is conducting and the DFIG injects power to the dc grid.

B. Mathematical Model

As shown in Fig. 1, the reference direction of stator current and rotor current is defined in terms of the generator mode. According to the equivalent circuit of the DFIG under the synchronized *d–q* reference frame, the air gap flux vector can be

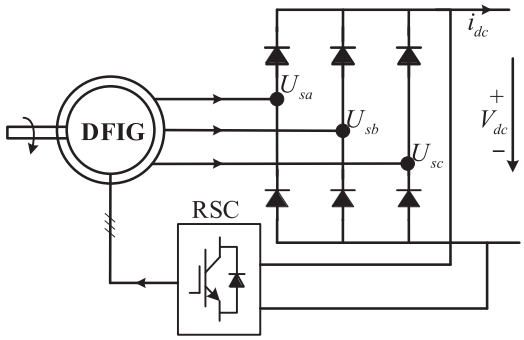

Fig. 1. Configuration of the DFIG-dc system. Diode bridge on the stator side and PWM converter on the rotor side.

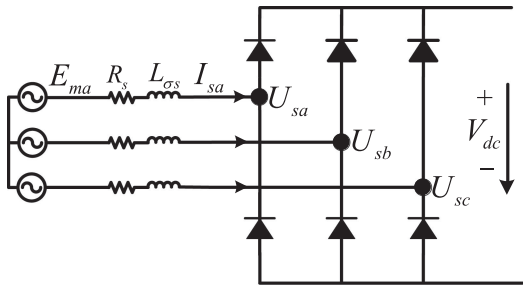

Fig. 2. Steady-state equivalent circuit of the DFIG-dc system.

expressed as

$$\boldsymbol{\psi}_{mdq} = L_m\left(-\boldsymbol{I}_{sdq} + \boldsymbol{I}_{rdq}\right) \tag{1}$$

where $\boldsymbol{\psi}_{mdq}$ is the air gap flux vector, $\boldsymbol{I}_{sdq}$ and $\boldsymbol{I}_{rdq}$ are the stator and rotor current vectors, respectively, and L_m is the mutual magnetic inductance.

In the steady state, the air gap EMF can be given as

$$\boldsymbol{E}_{mdq} = j\omega_s\boldsymbol{\psi}_{mdq} \tag{2}$$

where ω_s is the stator frequency.

Seen from the air gap side, the steady-state equivalent circuit of the DFIG-dc system can be seen as Fig. 2, where R_s is the stator resistance and $L_{\sigma s}$ is the stator leakage inductance.

When the diode bridge is working at the continuous conduction mode, the stator voltage is a three-step square wave and the magnitude of stator fundamental voltage can be calculated as [8]

$$U_{s1} = \frac{2}{\pi}V_{\rm dc}. \tag{3}$$

According to (3), the stator fundamental voltage is a fixed value since the dc-link voltage is constant. Thus, the stator voltage can be considered as a constant voltage source when ignoring the harmonics. The stator resistance is much smaller compared with the electrical impedance of leakage inductance and it can be ignored. The power transferred from the DFIG to the dc grid can be described as Fig. 3(a) and the phasor diagram can be seen as Fig. 3(b). The phasor diagram is in the synchronous *d–q* frame. The phase angle between the stator fundamental voltage vector and the air gap EMF vector is δ. Moreover, the

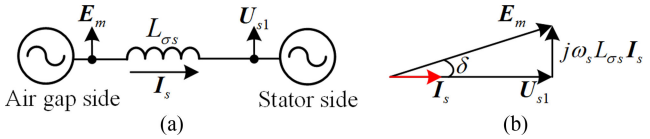

Fig. 3. Equivalent phasor diagram of the DFIG-dc system. (a) Equivalent diagram of power transfer. (b) Phasor diagram.

stator fundamental current vector is the same phase with the stator voltage vector due to the diode bridge [5]. The amplitude of the air gap EMF vector is E_m. Thus, the stator active power transferred from the DFIG to the dc grid can be calculated as

$$P_s = \frac{E_m U_{s1}}{\omega_s L_{\sigma s}} \sin\delta = \frac{\psi_m U_{s1}}{L_{\sigma s}} \sin\delta. \tag{4}$$

Since the stator leakage inductance is small, the amplitude of air gap EMF is almost the same as the stator fundamental voltage. The stator active power can be controlled by the phase angle between the air gap EMF and the stator voltage vector, which can be used for obtaining the stator frequency and the orientation angle in the system.

The stator active power is calculated by the dot product of stator voltage vector and stator current vector

$$P_s = \mathrm{Re}\left(\boldsymbol{U}_{sdq} \cdot \boldsymbol{I}_{sdq}\right) = U_{sd} I_{sd} + U_{sq} I_{sq}. \tag{5}$$

The torque can be calculated by the cross product of the air gap flux and conjugate of rotor current as

$$T_e = \mathrm{Re}\left(j\boldsymbol{\psi}_{mdq} \times \hat{\boldsymbol{I}}_{rdq}\right) = L_m \left(I_{sq} I_{rd} - I_{sd} I_{rq}\right). \tag{6}$$

The harmonic components existed in both the stator and rotor current result in the torque ripple. The detailed expression of torque ripple has been deduced in [15], which is not discussed in this article.

III. Control Strategy

Since the dc voltage is constant, the control objective of the RSC is to achieve the accurate regulation of output power to the dc grid. Furthermore, the stator frequency of the DFIG is not imposed by the ac grid, which also needs to be controlled additionally.

The RSC control scheme for the stator power and the stator frequency regulation is shown as Fig. 4, which mainly consists of the stator power control, stator frequency control, air gap flux orientation, and current control. The current control is the inner control loop, which is the same as the conventional current control and not repeated here. The stator power control, stator frequency control and air gap flux orientation, the improved direct resonant control, which will be elaborated in detail in the following three parts.

A. Stator Power Control

As can be seen from (4), the stator power will increase with higher angle δ, which is the integral of rotating speed deviation between the air gap EMF and the stator voltage vector. Besides,

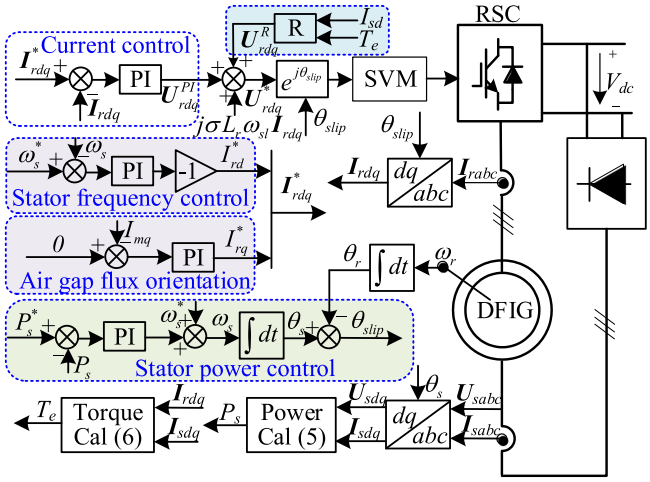

Fig. 4. RSC control scheme for the power and frequency regulation.

as the angle δ will increase with the higher stator frequency, the stator frequency can be generated by the power control loop as

$$\omega_s = \frac{k_{pp} s + k_{ip}}{s} \left(P_s^* - P_s\right) \tag{7}$$

where k_{pp} and k_{ip} are, respectively, the proportional gain and the integral gain of the power loop controller.

The orientation angle is the integral of stator frequency, which can be expressed as

$$\theta_s = \frac{1}{s} \omega_s. \tag{8}$$

B. Stator Frequency Control and Air Gap Flux Orientation

According to the air gap flux expressed in (1), the q-axis exciting current corresponding to the q-axis air gap flux can be expressed as

$$I_{mq} = I_{rq} - I_{sq}. \tag{9}$$

In order to achieve the air gap flux orientation, the q-axis air gap flux should be controlled to zero. Thus, the reference of q-axis rotor current can be expressed as

$$I_{rq}^* = \frac{k_{pf} s + k_{if}}{s} \left(0 - I_{mq}\right) \tag{10}$$

where k_{pf} and k_{if} are, respectively, the proportional gain and the integral gain of the q-axis exciting current controller.

Since the air gap flux vector is orientated in the d-axis, the magnitude of stator flux can be approximately calculated as

$$|\boldsymbol{\psi}_s| \approx |\boldsymbol{\psi}_m| = L_m \left(I_{rd} + |\boldsymbol{I}_s| \sin\delta\right) \approx L_m I_{rd}. \tag{11}$$

Since the product of stator frequency and stator flux is the magnitude of stator fundamental voltage, according to (3) and (11), the relationship between the d-axis rotor current and the stator frequency can be expressed as

$$\omega_s \approx \frac{2V_{\mathrm{dc}}}{\pi L_m I_{rd}}. \tag{12}$$

As can be seen from (12), the stator frequency is the inverse ratio with the d-axis rotor current. Thus, the reference of the

d-axis rotor current can be given as

$$I_{rd}^{*} = -\frac{k_{pf}s + k_{if}}{s}\left(\omega_s^{*} - \omega_s\right) \tag{13}$$

where k_{pf} and k_{if} are, respectively, the proportional gain and the integral gain of the stator frequency controller, which are the same as the q-axis exciting current controller since these two loops are both outer loops for generating the rotor current reference.

C. Improved Direct Resonant Control

The detailed mathematical model of the DFIG-dc system is built in [15], and the dominant harmonics in the air gap flux and stator current are fifth and seventh harmonics. Thus, the main torque ripple becomes sixth-order harmonic and a resonant controller can be applied to mitigate the torque ripple. The repetitive controller can also be applied to suppress all the torque ripples if all harmonics are considered. In this article, only a resonant controller is applied since it is just to prove that the direct resonant control strategy can also be used in this novel power-angle control strategy.

The transfer function of the resonant controller used in this article can be expressed as

$$G_R(s) = \frac{2k_r\omega_c s}{s^2 + 2\omega_c s + (6\omega_s)^2} \tag{14}$$

where ω_c is the cutoff frequency and k_r is the gain of the resonant controller. The cutoff frequency is applied to take the stator frequency fluctuation into account, the range of which is always designed from 5 to 15 rad/s. It is noted that 10 rad/s is used in this article.

The rotor harmonic voltage for mitigating the torque ripple and harmonic currents can be expressed as

$$\boldsymbol{U}_{rdq}^{R} = G_R(s)\left(I_{sd}^{*} - I_{sd}\right) + jG_R(s)\left(T_e^{*} - T_e\right). \tag{15}$$

In (15), both the I_{sd}^{*} and T_e^{*} are set as zero to mitigate the d-axis stator harmonic current and torque ripple.

Finally, the total rotor voltage reference can be expressed as

$$\boldsymbol{U}_{rdq}^{*} = \boldsymbol{U}_{rdq}^{\mathrm{PI}} + \boldsymbol{U}_{rdq}^{R} + j\sigma L_r\omega_{\mathrm{sl}}\boldsymbol{I}_{rdq} \tag{16}$$

where $\boldsymbol{U}_{rdq}^{\mathrm{PI}}$ is the output of the proportional and integral (PI) controller and $\boldsymbol{U}_{rdq}^{R}$ is the output of the direct resonant controller. ω_{sl} is the slip angular speed, σ is the leakage coefficient, and $j\sigma L_r\omega_{\mathrm{sl}}\boldsymbol{I}_{rdq}$ is the cross-coupling term, which is used as a feedforward item.

IV. Control Performance Analysis

The RSC control scheme in Fig. 4 indicates that the stator frequency and the stator power are nondecoupling control. The stator frequency is obtained by the power control loop. Thus, in order to analyze the control performance and stability of the power control loop and the stator frequency control loop, these two loops should be considered together.

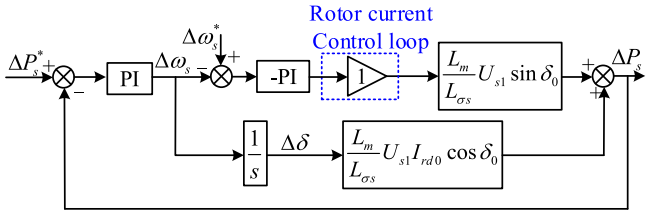

Fig. 5. Block diagram of the power and stator frequency control loop.

A. Stability of Stator Frequency and Power Control

According to (4), the stator active power can be expressed by stator voltage and d-axis rotor current as

$$P_s = \frac{\psi_m U_{s1}}{L_{\sigma s}}\sin\delta \approx \frac{L_m U_{s1}}{L_{\sigma s}} I_{rd}\sin\delta. \tag{17}$$

As can be seen from (17), the stator power is related to both the d-axis rotor current and angle δ. The effect of these two factors on the stator power can be expressed by the partial derivative as

$$\frac{\partial P_s}{\partial I_{rd}} = \frac{L_m}{L_{\sigma s}}U_{s1}\sin\delta \tag{18}$$

$$\frac{\partial P_s}{\partial \delta} = \frac{L_m}{L_{\sigma s}}U_{s1}I_{rd}\cos\delta. \tag{19}$$

Since the relationship between the stator power and angle δ is nonlinear, a small-signal model is deduced for the stability and control performance analysis. Assume that the steady-state working points are P_{s0}, δ_0, and I_{rd0}, the small-signal model of power can be expressed as

$$\Delta P_s = \left(\frac{L_m}{L_{\sigma s}}U_{s1}I_{rd}\cos\delta_0\right)\Delta\delta + \left(\frac{L_m}{L_{\sigma s}}U_{s1}\sin\delta_0\right)\Delta\left|I_{rd}\right|. \tag{20}$$

The relationship between the stator frequency and angle δ can be expressed as

$$\Delta\delta = \frac{1}{s}\Delta\omega_s. \tag{21}$$

Since the inner loop of the rotor current control is faster than the outer power control loop, it can be simplified as a unity gain block. Combining (20) and (21), the block diagram of the power control loop can be shown as Fig. 5.

According to Fig. 5, the characteristic equation of the power and stator frequency control system can be deduced as

$$G_{\mathrm{open}} = 1 + \frac{L_m U_{s1}}{L_{\sigma s}}\frac{k_{pp}s + k_{ip}}{s} \times \left(\frac{k_{pf}s + k_{if}}{s}\sin\delta_0 + \frac{1}{s}I_{rd0}\cos\delta_0\right). \tag{22}$$

Since the range of angle δ is quite small and near zero, $\sin\delta$ is approximately zero during the whole power range. According to Fig. 5, the effect of the stator frequency control on the power control can be eliminated. Thus, the operating point for designing the power control is the zero output power, which means that the angle δ is zero and $\sin\delta$ is zero. In this way, the power control loop can be simplified, as shown in Fig. 6.

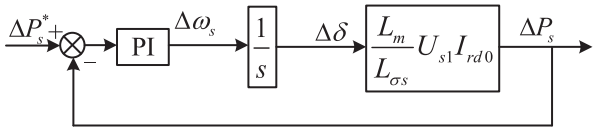

Fig. 6. Block diagram of the simplified power control loop.

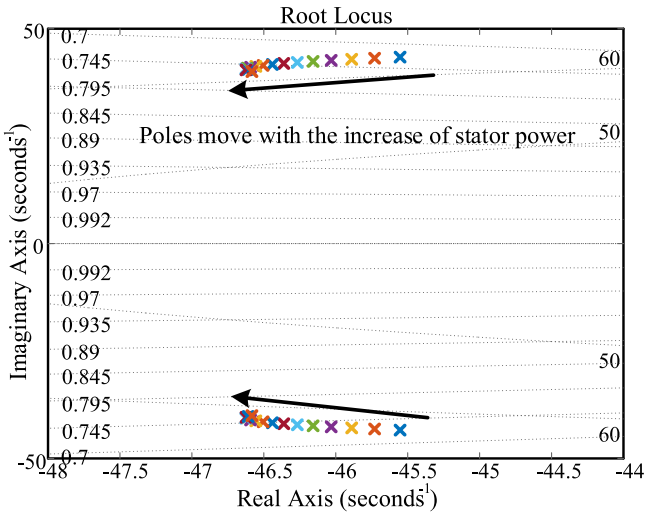

Fig. 7. Root locus of the stator power and frequency control loop when stator power changes from 0 to 1 p.u.

The transfer function of the stator power control loop can be deduced as

$$\frac{\Delta P_s}{\Delta P_s^*} = \frac{ak_{pp}s + ak_{ip}}{s^2 + ak_{pp}s + ak_{ip}} = \frac{2\xi\omega_n s + \omega_n^2}{s^2 + 2\xi\omega_n s + \omega_n^2} \tag{23}$$

where $a = L_m/L_{\sigma s} \cdot U_{s1} I_{rd0}$. As can be seen from the transfer function of the power loop, it is a second-order system. According to the design principle of a second-order system, the damping ratio ξ is always set as 0.707 and the bandwidth is designed based on the power control requirement. In this article, the bandwidth of the stator power control is designed as 10 Hz. Thus, the ω_n is set as 20π rad/s. The proportional (k_{pp}) and integral (k_{ip}) parameters of the power control loop can be obtained as 0.29 and 126, respectively. The proportional (k_{pf}) and integral (k_{if}) parameters of the stator frequency control loop are set as 1 and 80, respectively.

According to the characteristic equation listed in (22), the root locus of stator power changing from 0 to 1 p.u. is plotted in Fig. 7. The numbers smaller than 1 on the left side show the damping ratio ξ and the numbers on the right side represent the magnitude of the poles. It is obvious to see that the poles move to the left side with the increase of stator power and all the poles are located in the left-half plane, which indicates that the power and stator frequency control loop is always stable. Furthermore, the variation of poles with the stator power is not so significant, which indicates that the operating point has a little effect on the power control performance. In order to further validate this viewpoint, the step response with different stator power operating points is shown in Fig. 8. The blue line is the step response of a transfer function (23) and the red line is the simulation result of a real model. The step response of different power changes is consistent with the deduced transfer function from Fig. 6, which also corroborates with the root locus in Fig. 7.

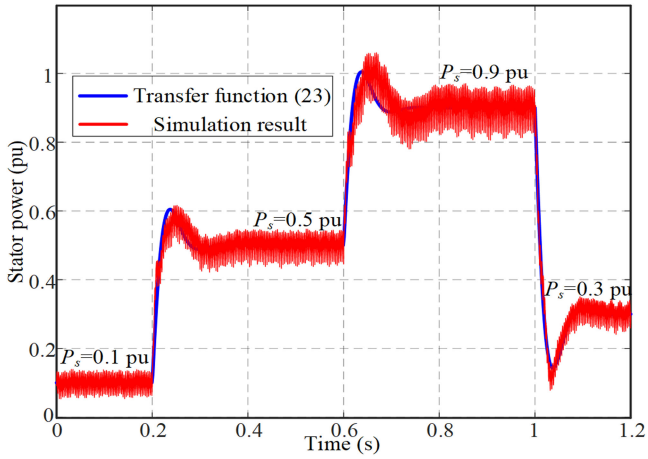

Fig. 8. Step response of different stator power change.

B. *Effectiveness of Improved Direct Resonant Control*

When the air gap flux vector is orientated at the d-axis, the q-axis air gap flux Ψ_{mq0} is equal to zero. Thus, the torque expression in (6) can be expressed in detail as

$$\begin{aligned} T_e = {} & (\psi_{md0} I_{rq0}) + (\psi_{md0} I_{rq6} + I_{rq0}\psi_{md6} - I_{rd0}\psi_{mq6}) \\ & + (\psi_{md6} I_{rq6} - \psi_{mq6} I_{rd6}) \end{aligned} \tag{24}$$

where Ψ_{md0} and Ψ_{mq0} express the air gap fundamental flux in the d–q axis, and Ψ_{md6} and Ψ_{mq6} express the sixth-order air gap harmonic flux in the d–q axis. I_{rd0} and I_{rq0} express the rotor fundamental flux in the d–q axis, and I_{rd6} and I_{rq6} express the sixth-order rotor harmonic current in the d–q axis.

The first term is an average torque, which is a constant dc value. The second term is the harmonic components with different frequencies. The third term is the product of smaller items that can be ignored. Thus, the dominant sixth-order torque ripple can be expressed as

$$T_{e6} = \psi_{md0} I_{rq6} + I_{rq0}\psi_{md6} - I_{rd0}\psi_{mq6}. \tag{25}$$

As can be seen from (24), the torque ripple is only affected by the q-axis rotor harmonic currents and has no relationship with the d-axis rotor harmonic currents. Thus, the direct resonant control on the q-axis can still be applied for mitigating torque ripple under the air gap flux orientation control.

The relationship of stator harmonic current and rotor harmonic current can be expressed as

$$I_{sd6} = I_{rd6} - \frac{1}{L_m}\psi_{md6} \tag{26}$$

where I_{sd6} expresses the sixth-order stator harmonic current in the d-axis.

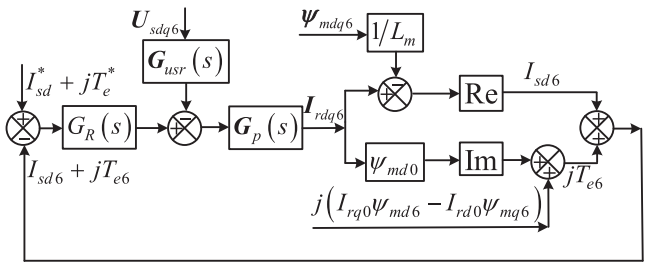

Fig. 9. Block diagram of improved direct resonant control.

Since the stator harmonic current is linear with the rotor harmonic current, the resonant controller can be used to control the rotor harmonic current, indicating that the resonant controller can also be used to directly control the stator harmonic current. Thus, the *d*-axis stator harmonic current and torque ripple can be combined as a new complex variable. The direct resonant control of the new complex variable can be expressed as the transfer function, as shown in Fig. 9.

The complex transfer function in Fig. 9 is obtained based on the DFIG model that can be expressed as

$$\boldsymbol{G}_{usr}(s) = \frac{L_m}{L_s}\frac{s + j\omega_{\mathrm{sl}}}{s + j\omega_s} \tag{27}$$

$$\boldsymbol{G}_p(s) = \frac{1}{R_r + \sigma L_r s} \tag{28}$$

where L_s is the stator inductance and R_r is the rotor resistance. As can be seen from the plant transfer function $\boldsymbol{G}_p(s)$, there is no coupling term in the denominator since the coupling term has been added to the rotor voltage as feedforward in (16).

As can be seen from Fig. 9, the *d*-axis stator harmonic current can be calculated as

$$I_{sd6} = \mathrm{Re}\left(\begin{array}{c}\frac{G_R(s)G_p(s)}{1+G_R(s)G_p(s)}\left(I_{sd}^* + jT_e^*\right) \\ + \frac{\boldsymbol{G}_{usr}(s)G_p(s)}{1+G_R(s)G_p(s)}U_{sdq6} - \frac{1}{L_m}\psi_{mdq6}\end{array}\right). \tag{29}$$

Since there is no imaginary part contained in the plant transfer function $\boldsymbol{G}_p(s)$, the *d*-axis stator harmonic current can be simplified as

$$I_{sdh} = \frac{G_R(s)\,G_p(s)}{1 + G_R(s)\,G_p(s)}I_{sdh}^* + \mathrm{Re}\left(\frac{\boldsymbol{G}_{usr}(s)\,G_p(s)}{1 + G_R(s)\,G_p(s)}U_{sdqh} - \frac{1}{L_m}\psi_{mdqh}\right). \tag{30}$$

As can be seen from (30), the *d*-axis harmonic current has no relationship with the torque reference, which can validate the decoupling control of the *d*-axis harmonic current and torque ripple. On the other hand, only the *d*-axis harmonic current can be suppressed to zero since the *q*-axis harmonic current is used for mitigating the torque ripple that cannot be suppressed to zero. Thus, there is still some stator harmonic currents, and the detailed analysis of the stator and rotor harmonic currents of improved direct resonant control can be seen in [18].

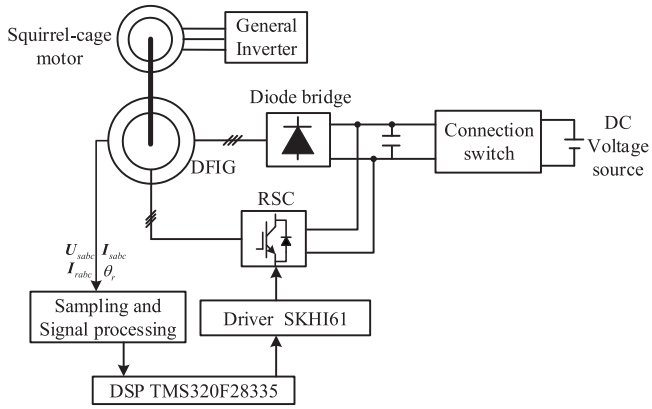

Fig. 10. Schematic diagram of the experimental system.

TABLE I
PARAMETERS OF THE TESTED DFIG

Parameters	*Value*	*Parameters*	*Value*
Rated power	1.0 kW	Rated voltage	110 V
Rated frequency	50 Hz	DC voltage	140 V
Pole pairs	3	R_s	1.01 Ω
R_r	0.88 Ω	L_m	87.5 mH
$L_{\sigma s}$	5.6 mH	$L_{\sigma r}$	5.6 mH

V. EXPERIMENTAL RESULTS

In order to validate the control strategy proposed in Section III, a DFIG-based experimental system is developed. The schematic diagram of the experimental system is shown in Fig. 10. The DFIG was driven by a squirrel cage induction motor with a general motor driver. The control strategy of the RSC is implemented on the TI TMS320F28335 DSP and the switching frequency is 10 kHz with a sampling frequency of 10 kHz. The parameters of the DFIG are given in Table I. All the waveforms are acquired by a YOKOGAWA DL750 scope.

The experimental results of stator flux orientation control in [9] with dc sampling offset in rotor current are shown in Fig. 11. The stator power reference is 400 W. The stator frequency reference is 50 Hz and the rotor speed is 800 r/min. Thus, the dc offset in rotor current is expressed as 10 Hz pulsation component in the synchronous *d*–*q* frame, which will cause 10 Hz ripples in stator power and torque. As can be seen from the results, the envelope of stator current oscillates at 10 Hz. The 10 Hz ripples in stator power and torque are even higher than the 300 Hz ripples that need to be suppressed.

In the latter experimental results, the novel power and frequency control method is applied. As can be seen from Fig. 12, the 10 Hz ripples are eliminated.

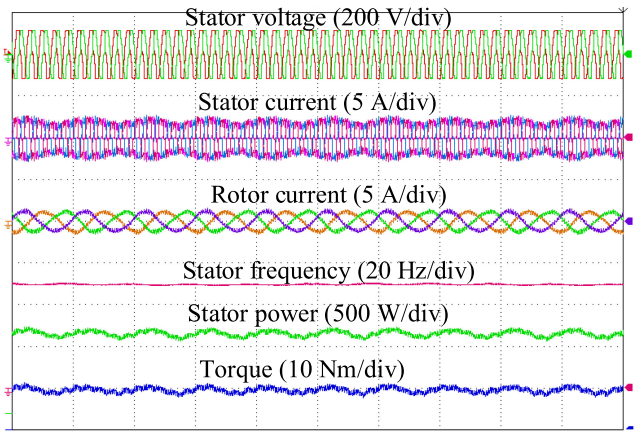

Fig. 11. Experimental results of the stator flux orientation control with dc offset.

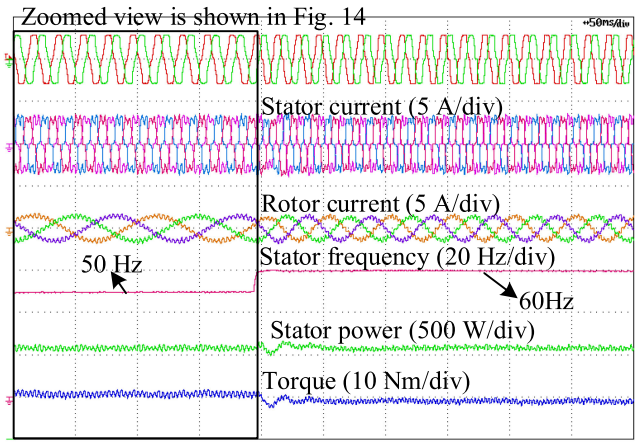

Fig. 13. Step response of stator frequency change from 50 to 60 Hz.

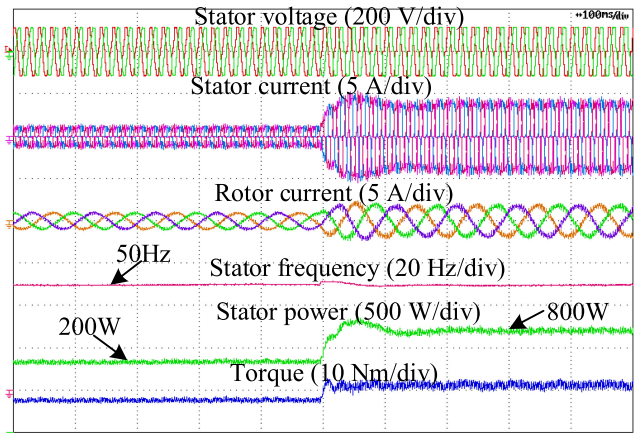

Fig. 12. Step response of power change from 200 to 800 W.

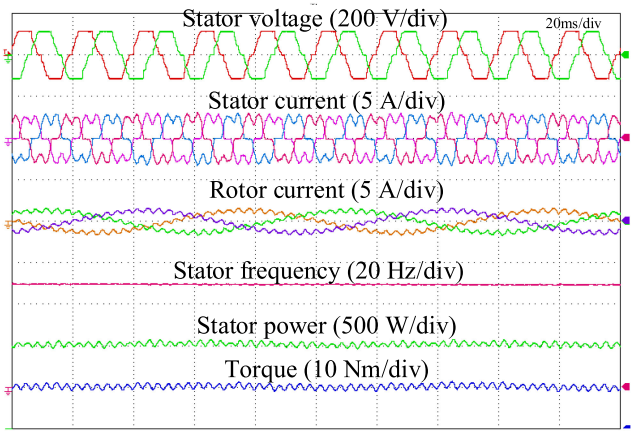

Fig. 14. Steady-state results without improved direct resonant control.

Fig. 12 shows the step response of DFIG when the stator active power reference changes from 200 to 800 W. The rotor speed is 800 r/min and the stator frequency is set as 50 Hz. The stator active power has a little overshoot since it is a second-order system, which is consistent with the theoretical analysis in Section IV-A. On the other hand, it can track the power reference accurately in 110 ms without the steady-state error, which validates the effectiveness of the stator power control loop.

The step response of the stator frequency change from 50 to 60 Hz is shown in Fig. 13. The stator power reference is 500 W. During the change of stator frequency, the stator power has a pulsation, which is caused by transient stator flux but will come to steady state in 50 ms. The stator frequency can quickly track the reference frequency in 10 ms without any overshoot that validates the effectiveness of the stator frequency control loop.

The zoomed view of the left part in Fig. 13 is shown in Fig. 14. The stator frequency is set as 50 Hz and the stator power is set as 500 W. Due to the diode bridge on the stator side, the stator current is highly distorted with fifth- and seventh-order harmonics, which are 23.7% and 6.4%, respectively. The 300 Hz ripples in the torque are 6.8%, which is harmful to the mechanical shaft of DFIG. Thus, it is necessary to mitigate the harmonic currents and torque ripple using an improved direct resonant control.

The steady-state results with improved direct resonant control are shown in Fig. 15. The fifth and seventh harmonic currents are both greatly reduced to 2.3% and 5.8%. The harmonic current cannot be totally suppressed due to the harmonic current necessary for reducing torque ripple. The 300 Hz torque ripple is also reduced to 0.93%. Thus, the improved direct resonant control can still be directly applied in the novel stator frequency and power control, which is simple and effective in mitigating both the torque ripple and harmonic currents. After mitigating the stator harmonic currents, the operation loss of DFIG is reduced and the efficiency of the DFIG-dc system is improved.

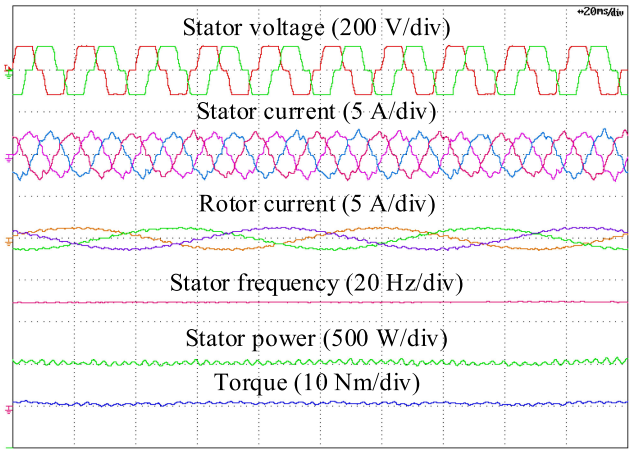

Fig. 15. Steady-state results with improved direct resonant control.

VI. Conclusion

A novel stator power and stator frequency control method of the DFIG-dc system based on the air gap flux orientation is proposed in this article. Instead of adopting the voltage model or current model for acquiring the stator frequency and orientation angle, the stator power control loop is applied for generating the stator frequency and orientation angle, which can avoid the parameter dependence and dc sampling offset effect. The air gap flux orientation method is achieved through controlling the q-axis exciting current to be zero. Furthermore, the improved direct resonant control for mitigating the torque ripple and harmonic currents can still be directly used, which indicates that the newly proposed control strategy is suitable for all the existing improved control strategies for suppressing harmonics or improving efficiency. This control strategy reduces parameter dependence without the loss of existing control performance.

References

[1] G. D. Marques and M. F. Iacchetti, "DFIG topologies for DC networks: A review on control and design features," *IEEE Trans. Power Electron.*, vol. 34, no. 2, pp. 1299–1316, Feb. 2019.
[2] T. Dragicevic, X. Lu, J. C. Vasquez, and J. M. Guerrero, "DC microgrids—Part I: A review of control strategies and stabilization techniques," *IEEE Trans. Power Electron.*, vol. 31, no. 7, pp. 4876–4891, Jul. 2016.
[3] N. Yu, H. Nian, and Y. Quan, "A novel DC grid connected DFIG system with active filter based on predictive current control," in *Proc. Int. Conf. Elect. Mach. Syst.*, Aug. 2011, pp. 4525–4537.
[4] H. Nian and X. Yi, "Coordinated control strategy for doubly-fed induction generator with dc connection topology," *IET Renewable Power Gener.*, vol. 9, no. 7, pp. 747–756, Sep. 2015.
[5] M. F. Iacchetti, G. D. Marques, and R. Perini, "Operation and design issues of a DFIG stator-connected to a DC net by a diode rectifier," *IET Electr. Power Appl.*, vol. 8, no. 8, pp. 310–319, Sep. 2014.
[6] G. D. Marques and M. F. Iacchetti, "Stator frequency regulation in a field oriented controlled DFIG connected to a DC link," *IEEE Trans. Ind. Electron.*, vol. 61, no. 11, pp. 5930–5939, Nov. 2014.
[7] G. D. Marques and M. F. Iacchetti, "Inner control method and frequency regulation of a DFIG connected to a DC link," *IEEE Trans. Energy Convers.*, vol. 29, no. 2, pp. 435–444, Jun. 2014.
[8] M. F. Iacchetti, G. D. Marques, and R. Perini, "Torque ripple reduction in a DFIG-DC system by resonant current controllers," *IEEE Trans. Power Electron.*, vol. 30, no. 8, pp. 4244–4254, Aug. 2015.
[9] H. Nian, C. Wu, and P. Cheng, "Direct resonant control strategy for torque ripple mitigation of DFIG connected to DC link through diode rectifier on stator," *IEEE Trans. Power Electron.*, vol. 32, no. 9, pp. 6936–6945, Sep. 2017.
[10] G. D. Marques and M. F. Iacchetti, "A self-sensing stator-current-based control system of a DFIG connected to a DC-link," *IEEE Trans. Ind. Electron.*, vol. 62, no. 10, pp. 6140–6150, Oct. 2015.
[11] C. Wu and H. Nian, "Sinusoidal current operation of DFIG-DC system without stator voltage sensors," *IEEE Trans. Ind. Electron.*, vol. 65, no. 8, pp. 6250–6258, Aug. 2018.
[12] C. Wu and H. Nian, "An improved repetitive control of DFIG-DC system for torque ripple suppression," *IEEE Trans. Power Electron.*, vol. 33, no. 9, pp. 7634–7644, Sep. 2018.
[13] H. Misra, A. Gundavarapu, and A. K. Jain, "Control scheme for DC voltage regulation of stand-alone DFIG-DC system," *IEEE Trans. Ind. Electron.*, vol. 64, no. 4, pp. 2700–2708, Apr. 2017.
[14] H. Misra and A. K. Jain, "Analysis of stand-alone DFIG-DC system and DC voltage regulation with reduced sensors," *IEEE Trans Ind. Electron.*, vol. 64, no. 6, pp. 4402–4412, Jun. 2017.
[15] H. Misra and A. K. Jain, "Mathematical modelling and control of standalone DFIG-DC system in rotor flux reference frame," *IEEE Trans. Ind. Electron.*, vol. 65, no. 5, pp. 3708–3719, May 2018.
[16] G. D. Marques and M. F. Iacchetti, "Minimization of torque ripple in the DFIG-DC system via predictive delay compensation," *IEEE Trans. Ind. Electron.*, vol. 65, no. 1, pp. 103–113, Jan. 2018.
[17] S. M. A. Cruz, G. D. Marques, P. F. C. Goncalves, and M. F. Iacchetti, "Predictive torque and rotor flux control of a DFIG-DC system for torque ripple compensation and loss minimization," *IEEE Trans. Ind. Electron.*, vol. 65, no. 12, pp. 9301–9310, Dec. 2018.
[18] C. Wu and H. Nian, "Improved direct resonant control for suppressing torque ripple and reducing harmonic current losses of DFIG-DC system," *IEEE Trans. Power Electron.*, vol. 34, no. 9, pp. 8739–8748, Sep. 2019.

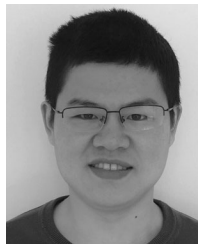

Chao Wu (Member, IEEE) was born in Hubei Province, China. He received the B.Eng. degree from the Hefei University of Technology, Hefei, China, in 2014, and the Ph.D. degree from Zhejiang University, Hangzhou, China, in 2019, both in electrical engineering.

He is currently a Postdoctoral Researcher with the Department of Energy Technology, Aalborg University, Aalborg, Denmark. His current research interests include cooperative control of multiconverter systems, particularly the control and operation of doubly fed induction generators for dc connection.

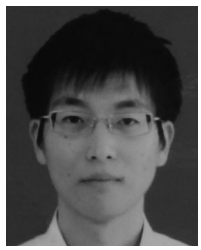

Dao Zhou (Senior Member, IEEE) received the B.S. degree from Beijing Jiaotong University, Beijing, China, in 2007, the M.S. degree from Zhejiang University, Hangzhou, China, in 2010, and the Ph.D. degree from Aalborg University, Aalborg, Denmark, in 2014, all in electrical engineering.

Since 2014, he has been with the Department of Energy Technology, Aalborg University, where he is currently an Assistant Professor. His research interests include modeling, control, and reliability of power electronics in renewable energy applications.

Dr. Zhou was a recipient of the Renewable and Sustainable Energy Conversion Systems of the IEEE Industry Applications Society First Prize Paper Award in 2015 and the Best Session Paper at Annual Conference of the IEEE Industrial Electronics Society (IECON) in Austria in 2013.

Peng Cheng (Member, IEEE) was born in Liaoning Province, China. He received the B.S. and Ph.D. degrees in electrical engineering from Zhejiang University, Hangzhou, China, in 2011 and 2016, respectively.

He is currently an Assistant Professor with the Department of China Institute of Energy and Transport Integration Development, North China Electric Power University, Beijing, China. His current research interests include multiconverter power systems and renewable power generation, particularly wind power generation.

Frede Blaabjerg (Fellow, IEEE) received the Ph.D. degree in electrical engineering from Aalborg University, Aalborg, Denmark, in 1995.

From 1987 to 1988, he was with ABB-Scandia, Randers, Denmark. He became an Assistant Professor in 1992, an Associate Professor in 1996, and a Full Professor of power electronics and drives in 1998. Since 2017, he has been a Villum Investigator. He is honoris causa with University Politehnica Timisoara, Timisoara, Romania, and Tallinn University of Technology, Tallinn, Estonia. His current research interests include power electronics and its applications, such as in wind turbines, PV systems, reliability, harmonics, and adjustable speed drives. He has authored or coauthored more than 600 journal papers in the fields of power electronics and its applications. He is the coauthor of four monographs and editor of ten books in power electronics and its applications.

Dr. Blaabjerg was a recipient of 32 IEEE Prize Paper Awards, the IEEE PELS Distinguished Service Award in 2009, the EPE-PEMC Council Award in 2010, the IEEE William E. Newell Power Electronics Award 2014, the Villum Kann Rasmussen Research Award 2014, the Global Energy Prize in 2019, and the 2020 IEEE Edison Medal. From 2006 to 2012, he was the Editor-in-Chief of the IEEE TRANSACTIONS ON POWER ELECTRONICS. He was a Distinguished Lecturer for the IEEE Power Electronics Society from 2005 to 2007 and for the IEEE Industry Applications Society from 2010 to 2011 as well as from 2017 to 2018. From 2019 to 2020, he was a President of the IEEE Power Electronics Society. He is a Vice-President of the Danish Academy of Technical Sciences too. He was nominated in 2014–2019 by Thomson Reuters to be between the 250 most cited researchers in Engineering in the world.